



# Corrosion study of graphene oxide coatings on AZ31B magnesium alloy

Muhammad Faheem Maqsood, Mohsin Ali Raza, Faizan Ali Ghauri, Zaem Ur Rehman, Muhammad Tasadaq Ilyas

© American Coatings Association 2020

**Abstract** The aim of this study was to produce graphene oxide (GO) coatings on biodegradable AZ31B magnesium (Mg) alloy. GO was synthesized by improved Hummers' method, and a suspension was prepared in deionized water by ultrasonication. GO coatings were developed on AZ31B Mg alloy by electrophoretic deposition (EPD). The EPD parameters, such as voltage and time, were optimized to obtain uniform GO coatings. Characterization was carried out using Fourier transform infrared spectroscopy, X-ray diffraction, atomic force microscopy (AFM), and scanning electron microscopy. GO was found to have a thickness of approximately 0.7–1 nm as determined by AFM. Electrochemical behavior of coatings was evaluated by Tafel analysis and electrochemical impedance spectroscopy (EIS) in Ringer's lactate solution. GO coatings improved the corrosion resistance of the AZ31B Mg alloy by 16× in Ringer's lactate solution as compared to bare Mg alloy.

**Keywords** Magnesium alloys, Improved Hummers' method, Graphene oxide, Coatings, Atomic force microscopy, Ringer's lactate, Corrosion

## Introduction

Magnesium (Mg) and its alloys have attained much attention due to their unique combination of properties, i.e., low specific gravity, specific strength, high rigidity, dimensional stability, and good machinability.<sup>1–3</sup> Mg and its alloys are suitable materials for numerous applications in the field of transportation,

aerospace, electronics, etc.<sup>4</sup> Moreover, their Young's modulus and compression strength are comparable to natural bone, which make them potentially useful for biomedical implant applications.<sup>5</sup> Mg is needed for many biochemical reactions in the body; therefore, its biodegradation causes no tissue loss or damage to the body. Being nontoxic, Mg plays a supporting role in the growth of tissues, unlike nonbiodegradable permanent metallic implants that produce physical irritation in the body and have poor adaptability to tissue growth.<sup>6,7</sup>

A notable disadvantage of Mg metal in many engineering applications is its high electrochemical activity (low corrosion resistance) especially in aqueous environments. However, this is a significant advantage for biodegradable medical implants. Currently, acceptable metallic biomaterials include stainless steels, titanium, and cobalt–chromium-based alloys.<sup>8</sup> These metallic biomaterials are limited in their use as body implants due to possible release of toxic metallic ions and/or particles in the body via corrosion or wear processes. Mg alloy-based body implants have an advantage over these alloys as their in vivo corrosion results in the release of soluble, nontoxic ions that are not only harmless to the body but also have a beneficial effect on the growth of new bone tissues.<sup>9,10</sup>

Chaya et al.<sup>11</sup> studied in vivo Mg degradation and found a corrosion rate of 0.40 mm/year after 8 weeks of immersion. They argued that fractured bone healing starts by 8 weeks and reaches maturation after 16 weeks. The minimum degradation rate required for the common metallic implants, i.e., stainless steel and titanium, is 12 weeks, and this means that the rate of dissolution of Mg in the presence of chloride, bromide, and sulfate-containing environments, such as the human body, needs to be reduced.<sup>12</sup>

Biodegradation of Mg alloys can be tuned to the desired level by controlling the corrosion rate with the application of suitable coatings such as hydroxyapatite,

M. F. Maqsood, M. A. Raza, F. A. Ghauri, Z. U. Rehman (✉), M. T. Ilyas  
Department of Metallurgy and Materials Engineering,  
University of the Punjab, Lahore, Pakistan  
e-mail: zaemurrehman6@gmail.com

epoxy silane, and graphene. These coatings can be developed by various available techniques such as chemical conversion, electrophoretic deposition (EPD), anodic oxidation, physical vapor deposition (PVD), and chemical vapor deposition (CVD).<sup>13–18</sup> The performance of coatings relies on the better adhesion of coatings on the substrate, absence of defects, adequate thickness, uniformity, adequate flexibility, and toughness to withstand impacts.

Graphene<sup>19</sup> has been applied in various biotechnology applications due to its biostability, nontoxicity, extremely large surface area, and good electrical and mechanical properties.<sup>20–22</sup> Graphene derivatives, graphene oxide (GO) with oxygen containing functional groups such as hydroxyl, epoxide, carboxyl, and carbonyl groups, enable its dispersion in water to form stable suspensions.<sup>23</sup>

Few reports demonstrate that graphene and GO coatings are useful in protecting metallic substrates against corrosion.<sup>24</sup> Prasai et al.<sup>25</sup> presented that a coating of graphene deposited by CVD process retards the corrosion rate of copper 7× and for nickel almost 20×. EPD is a versatile and easy technique to develop GO coatings on metallic substrates and is comparable to high-temperature CVD grown coatings. An et al.<sup>26</sup> reported GO coating developed by EPD on the surface of the stainless steel. He et al.<sup>27</sup> fabricated GO films on sintered NdFeB magnets uniformly by EPD and studied their corrosion behavior. They measured the decrease in corrosion current density and the positive shift in corrosion potential which suggest that GO films acted as a corrosion inhibitor. Recently, Raza et al.<sup>28</sup> showed that GO-EPD coatings on Cu lowered the corrosion rate of Cu by 6× compared to that of bare Cu. In this study, we used EPD technique to produce GO coatings on biodegradable AZ31B Mg alloy, and the corrosion behavior of GO-coated Mg in Ringer's lactate solution was studied using Tafel analysis and electrochemical impedance spectroscopy (EIS).

## Experimental

### Materials

Graphite powder (particle size 10 μm) was obtained from Asbury Graphite Mills, USA, and used as a precursor for the production of GO. Analytical grade chemicals (KMnO<sub>4</sub>, H<sub>2</sub>SO<sub>4</sub>, H<sub>3</sub>PO<sub>4</sub>, ethanol, and H<sub>2</sub>O<sub>2</sub>) were used in this work. Suspension and solutions were prepared in deionized (DI) water.

### Graphite oxide synthesis

Improved Hummers' method<sup>29</sup> was used for the synthesis of graphite oxide. In a round-bottom flask, a mixture of H<sub>3</sub>PO<sub>4</sub>/H<sub>2</sub>SO<sub>4</sub> (40:360 mL) was mixed

with 3 g of graphite powder. Then, 18 g of KMnO<sub>4</sub> was slowly added to this mixture under continuous stirring. During the addition of KMnO<sub>4</sub>, exothermic reaction occurred which raised the temperature of the mixture to 35–40°C. The mixture was continuously stirred for 12 h. The stirred solution was left to cool to room temperature, followed by slow addition of 400 mL of DI water. Then, 3 mL of 30% H<sub>2</sub>O<sub>2</sub> was added to the final solution. Addition of H<sub>2</sub>O<sub>2</sub> resulted in a bright yellow color of the solution. The developed solution was filtered using conventional filter papers (Whatman No. 42). There was continuous washing of residue left on filter papers with 30% HCl, ethanol, followed by plenty of DI water, until pH of residue was neutralized. Finally, powder was dried overnight at 80°C in a vacuum oven.

### Sample preparation

Silicon carbide papers (grit size 320–1000) were used to grind Mg samples having dimensions 5 × 2 × 0.3 cm<sup>3</sup> to remove the oxide layer and to roughen the surface. Samples were ultrasonicated in ethanol for 5 min to remove any organic contaminants, followed by rinsing with DI.

### EPD coating

Graphite oxide was ultrasonicated in DI water (2 mg/mL) for 2 h at 35°C to form GO suspension for the coatings. Sonication caused exfoliation of graphite oxide that resulted in the GO formation. In EPD, cell platinum was used as cathode and Mg samples as an anode. Both electrodes were immersed in GO suspension at 1 cm distance and connected to a DC power supply. EPD coatings were produced using the cell shown in Fig. 1. EPD was conducted at different deposition times, 3 V for 30, 60, and 90 s, to obtain various GO coatings.

### Mechanism of GO deposition

Various research articles reported a mechanism of GO deposition. GO, being a negatively charged species, tends to deposit on a positively charged anode (Eqs. 1–2). An et al.<sup>26</sup> suggested that GO is partially reduced during the EPD deposition process. According to them, negatively charged carboxylate groups on the periphery of graphene will lose electrons upon reaching the surface of the anode (Eq. 4). Carboxylate groups oxidize and deposit on the surface of the anode (Eq. 5). Deposition of GO on the anode continues by the oxidative decarboxylation process (Eq. 5) until the whole dipped anode is fully covered with GO. During this process, due to Kolbe reaction, the graphene sheets having unpaired electrons as carboxylate groups reach the anode surface and release CO<sub>2</sub> (Eq. 5).

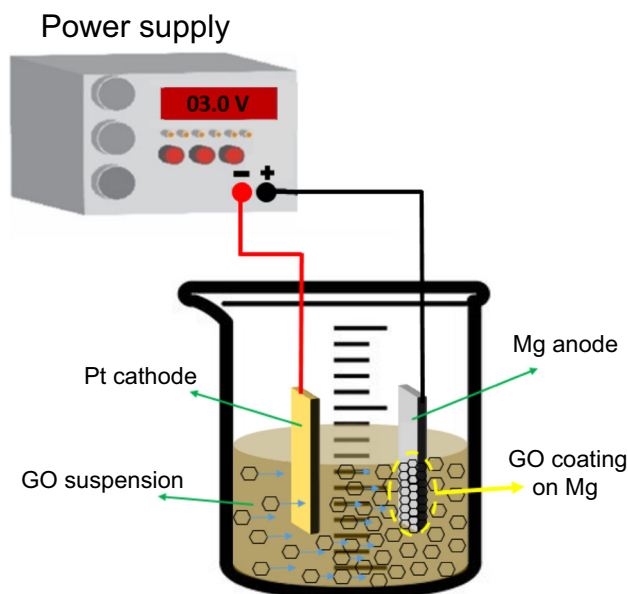
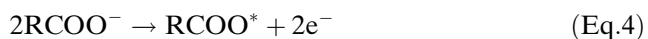
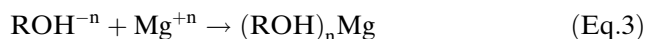


**Fig. 1: Schematic representation of EPD coating of GO on Mg**

These graphene sheets of unpaired electrons move freely in the GO framework at the anode surface and find other sheets with unpaired electrons to form covalent bonds.<sup>28</sup> With increased time or voltage, coating delamination starts.<sup>28</sup> Optimized parameters for deposition of GO coating on Mg, at which GO was not delaminated and remained adhered to the surface, were 3 V and 90 s.



where “R” refers to graphene sheets.

### Characterization

The thickness of GO sheets was measured by atomic force microscopy (AFM) (Nano-Solver, NT-MDT). One to two drops of diluted GO/water suspension were evaporated on a mica sheet, and AFM images were obtained using semicontact mode. The roughness of bare Mg and GO-coated Mg samples was measured on small samples using semicontact mode of AFM. Scanning electron microscopy [(SEM), (TESCAN Vega

LMU)] of bare Mg and EPD-GO-coated samples was performed to study the morphology and uniformity of GO coating.

X-ray diffraction [(XRD) (Equinox 2000, Thermo Fisher Scientific)] analysis of graphite oxide, bare Mg, and EPD-GO-coated Mg samples was performed using a powder diffractometer equipped with curved position sensitive detector. Diffraction patterns were obtained using  $\text{CuK}_{\alpha 1}$  radiation (produced with Ge monochromator) in the range of  $2\theta^\circ$  from 5 to  $80^\circ$  in real time for a total acquisition time of 10 min. Fourier transform infrared [(FTIR) (Agilent Cary 630)] spectrum of graphite oxide was obtained using attenuated total reflectance (ATR) mode to analyze the presence of functional groups.

### Corrosion study

To evaluate the corrosion behavior of GO coating, electrochemical tests were carried out in a three-electrode system using potentiostat/galvanostat/ZRA (Reference 3000, Gamry Instruments, USA). Bare and coated samples were designated as working electrode, graphite as a counter electrode, and saturated calomel electrode (SCE) as a reference electrode. Tests were performed in Ringer’s lactate solution. To measure corrosion rate, Tafel scan tests were performed in a potential range of  $-0.5$  to  $+0.5$  V versus open-circuit potential (OCP) at a scan rate of 3 mV/sec. To further evaluate the electrochemical behavior of Mg and EPD-GO-coated Mg, electrochemical impedance spectroscopy (EIS) was performed in the frequency range of 10 mHz–100 kHz with a potential perturbation of  $\pm 10$  mV.

## Results and discussion

### XRD

XRD pattern of graphite oxide is shown in Fig. 2. Diffraction peak of graphite oxide present at  $11.67^\circ$  corresponds to (001) plane, having d-spacing of ca. 0.85 nm as compared to d-spacing 0.32 nm of natural graphite, which shows successful oxidation of graphite.<sup>29</sup> XRD pattern of bare Mg and EPD-GO-coated samples is shown in Fig. 3. There were no (002) or (001) peaks of graphite or graphite oxide. The reduction in intensities of peaks due to GO coating was observed in EPD-GO-coated samples, which suggests GO deposition on Mg substrate.

### FTIR

FTIR analysis of GO is shown in Fig. 4. FTIR spectrum of GO has transmittance peaks at  $3382\text{ cm}^{-1}$ ,  $1726\text{ cm}^{-1}$ , and  $1621\text{ cm}^{-1}$ , which corre-

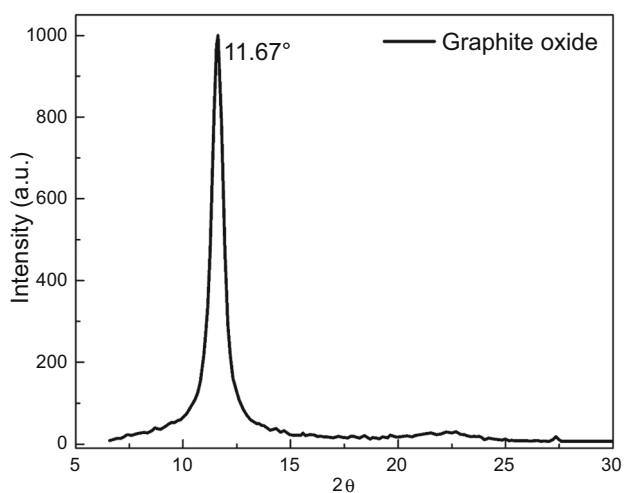


**Fig. 2:** XRD pattern of synthesized graphite oxide by improved Hummers' method

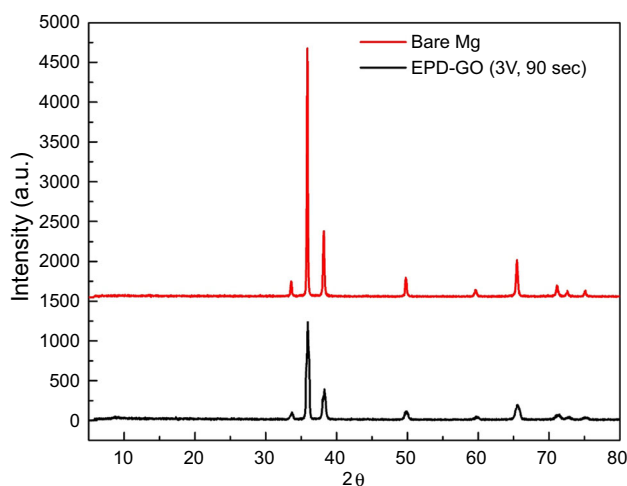


**Fig. 3:** XRD patterns of bare Mg and EPD-GO (3 V, 90 s)-coated Mg samples

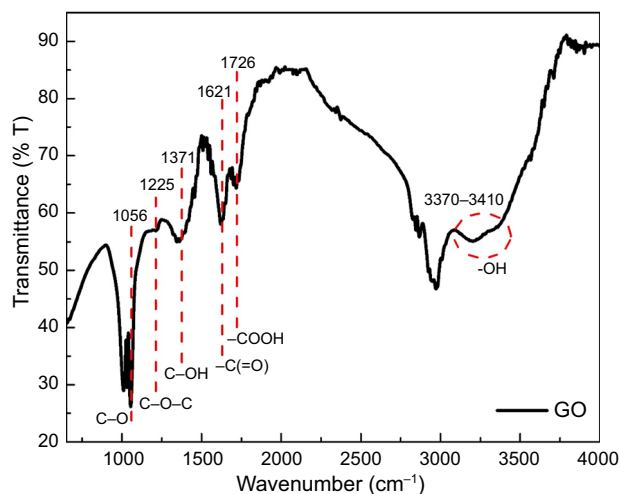


**Fig. 4:** FTIR spectrum of GO with its functional groups

spond to -OH, -COOH, and -C(=O) functional groups, respectively.<sup>30</sup> The presence of oxygen functional groups is evidence of successful oxidation of graphite.

### AFM

Semiconduct mode AFM image of GO sheets with height profile is presented in Fig. 5a. GO sheets have a thickness of 0.7–1 nm and lateral dimensions of ~ 500 nm, although some smaller sheets were also observed. To evaluate surface coverage of the coatings,<sup>31</sup> surface roughness of bare Mg and EPD-GO-coated Mg (3 V, 90 s) samples was measured by AFM.

Figure 5b–e shows bare Mg sample has a roughness of ca. Ra = 29 nm, which is higher than that of EPD-GO-coated Mg (3 V, 90 s) that has roughness of Ra = 9 nm. The smoother GO-coated Mg suggests GO coating is uniform and has provided better coverage to the underlying Mg substrate.

### SEM

To analyze the topography of the coatings, SEM images of bare Mg and EPD-GO-coated Mg (3 V, 90 s) samples are presented in Fig. 6. A bare sample had grinding marks due to roughness created deliberately to improve adhesion of GO coating with Mg substrate (Fig. 6a, b). On the other hand, EPD-GO (3 V, 90 s) sample had no cracks and GO fairly covered the grinding marks (Fig. 6c, d).

### Corrosion study

#### Tafel scan

To determine corrosion rate of coatings in Ringer's lactate solution, Tafel analysis was conducted. Figure 7 shows the Tafel curves of bare Mg and EPD-GO-coated Mg samples at 3 V for different coating times (30, 60, and 90 s). The Echem Analyst version 7.2 (Gamry Instruments) was used to calculate corrosion rates from the regions of the curves that conform to Butler–Volmer equation.

Corrosion potential  $E_{\text{corr}}$  tells about the corrosion susceptibility of the material under investigation. Tafel analysis revealed a positive shift in  $E_{\text{corr}}$  for coatings. However, larger (270 mV) shift in  $E_{\text{corr}}$  for EPD-GO (3 V, 90 s) demonstrates its decreased tendency toward corrosion compared to the bare Mg and EPD-GO (3 V for 30 and 60 s coating times). This positive shift is attributed to more uniformity and coverage of GO as determined by AFM and SEM analyses (Figs. 5, 6). The kinetic parameters along with their standard deviation obtained after Tafel fitting are presented in Table 1. EPD-GO (3 V, 90 s) coating



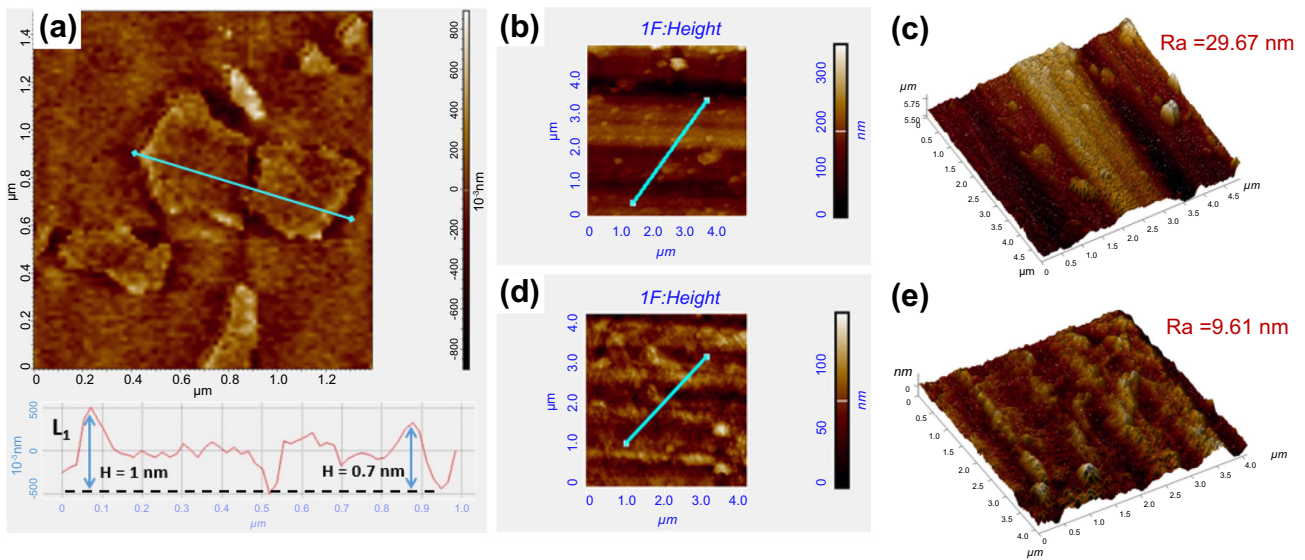


**Fig. 5:** a AFM image of GO along with height profile, b 2D profile of bare Mg, c 3-D profile of bare Mg 3-D along with roughness value, d 2D profile of EPD-GO-coated Mg (3 V, 90 s), and e 3-D profile of EPD-GO-coated Mg (3 V, 90 s) along with roughness value

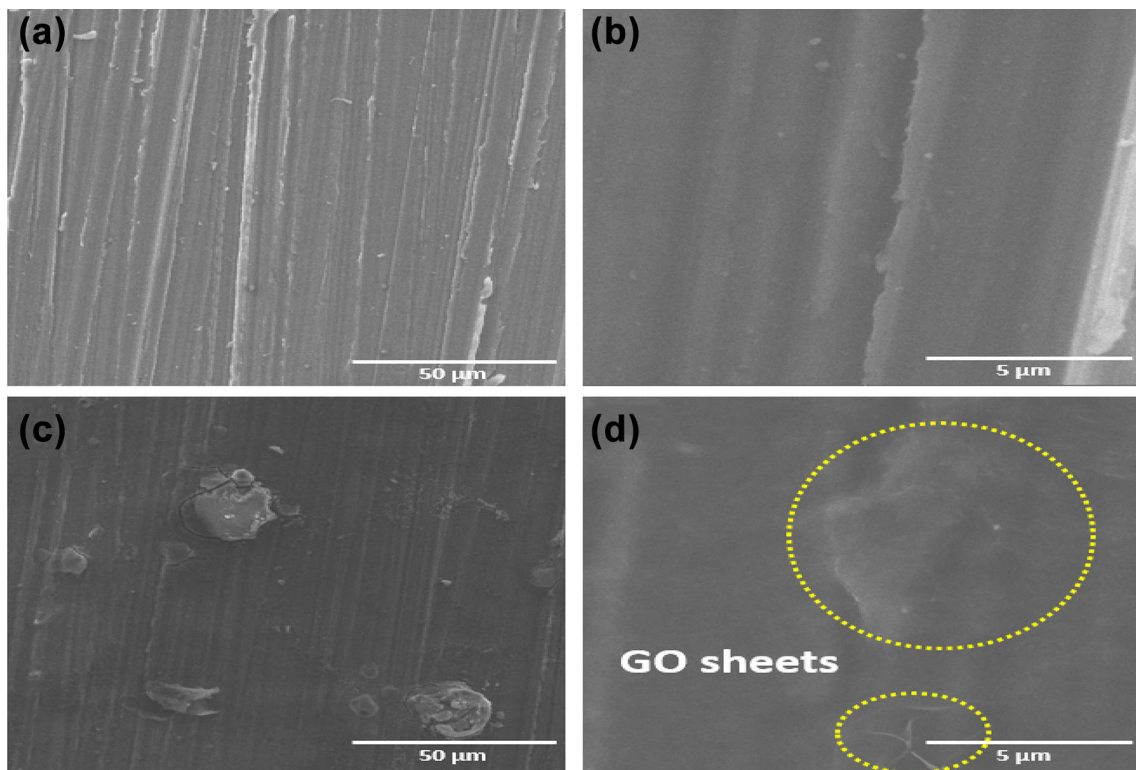


**Fig. 6:** SEM images (a and b) bare Mg and (c and d) EPD-GO (3 V, 90 s)-coated Mg

reduced corrosion rate of Mg alloy by ca. 16× compared to bare Mg. The GO coating acted as a physical barrier by creating a tortuous path in front of aggressive electrolyte ions and stopped them from reaching the metal surface.<sup>32,33</sup> The reduction in the corrosion rate of AZ31B Mg alloy reported here is comparable

with the previous studies.<sup>34,35</sup> To validate corrosion inhibition ability of EPD-GO determined by Tafel analysis, EIS was carried out to explain how corrosion inhibition improved due to GO coating.

**EIS**

EIS is a nondestructive technique used to determine impedance of the conductive samples that are in direct contact with the electrolyte.<sup>36</sup> Figure 8a shows Nyquist curves of bare Mg and EPD-GO-coated Mg samples in Ringer’s lactate. The curves display capacitive loops at high- and medium-frequency regimes, indicating double-layer phenomena due to the formation of a loosely bonded oxide layer on the surface of the samples.<sup>37</sup> On the other hand, inductive behavior in low-frequency regime is attributed to the relaxation mechanism of the adsorbed species when metal comes in contact with Ringer’s lactate solution containing many aggressive ion species such as chloride, fluoride, and sulfate.

Nyquist plots of all samples represent similar capacitive loops with different diameters, suggesting that a similar corrosion mechanism occurred for all samples but with different corrosion rates (as obtained in Tafel analysis).<sup>38</sup> EPD-GO (3 V, 90 s) has a larger diameter of capacitive loop due to adherent GO

coating which resisted the formation of nonadherent Mg(OH)<sub>2</sub> layer. To better understand the electrochemical response of the EPD-GO (3 V, 90 s), a simple electrochemical equivalent circuit (ECC) model was fitted (goodness of fit  $\leq 10^{-3}$ ) on experimental data to obtain circuit values<sup>39</sup> as shown in Fig. 8c. The obtained circuit values from fitted curves are presented in Table 2, where  $R_s$  is the solution resistance,  $R_{ct}$  is the resistance to charge transfer,  $R_{ad}$  is the resistance of adsorbed species,  $L$  is the inductance, and  $Y_o$  is the admittance.

EPD-GO (3 V, 90 s) had  $\sim 6\times$  higher  $R_{ct}$  (873.5  $\Omega\cdot\text{cm}^2$ ) than that of bare Mg (151.3  $\Omega\cdot\text{cm}^2$ ) which validated Tafel results. EPD-GO (3 V, 90 s) has the highest  $R_{ad}$  (299.3  $\Omega\cdot\text{cm}^2$ ) (resistance by adsorbed species), indicating compactness of the coating and possibility of electrolyte to form an adherent double layer that would resist further corrosion. Peng et al.<sup>34</sup> reported an improvement of  $\sim 6\times R_{ct}$  in the case of the hydroxyapatite/graphene oxide bilayer coatings over the bare AZ31 Mg alloy. The low  $Y_o$  admittance values of EPD-GO samples compared to bare Mg may be due to a swelling effect of the coating as partially reduced GO still has hydrophilic nature.<sup>16</sup> The equivalent inductive behavior observed for EPD-GO (3 V, 90 s) and bare Mg in the low frequency shows that the GO coatings are beneficial for tailoring the degradation rate of the Mg alloys without damaging underlying metal inherent properties.

Bode plots of bare Mg and EPD-GO-coated Mg samples at various coating parameters are shown in Fig. 8b. Bode plot shows impedance at various frequency ranges. At lower frequency, EPD-GO (3 V, 90 s) has the highest impedance of about 300  $\Omega\cdot\text{cm}^2$ , which is about  $4\times$  higher than that of bare Mg (80  $\Omega\cdot\text{cm}^2$ ). This indicates higher corrosion resistance of EPD-GO (3 V, 90 s) sample among other EPD-GO-coated samples that have relatively lower impedance at lower frequency, though greater than bare Mg.

It can be deduced from the corrosion tests that GO coatings on biodegradable Mg alloys can provide reasonable corrosion protection, which is desirable for the bioimplants to maintain their inherent properties during the bone healing stage. After deterioration of the coating, Mg alloys biodegrade as usual. Thus, GO coating can be an effective choice for the implants that require protection for certain time against corrosion caused by body fluids.

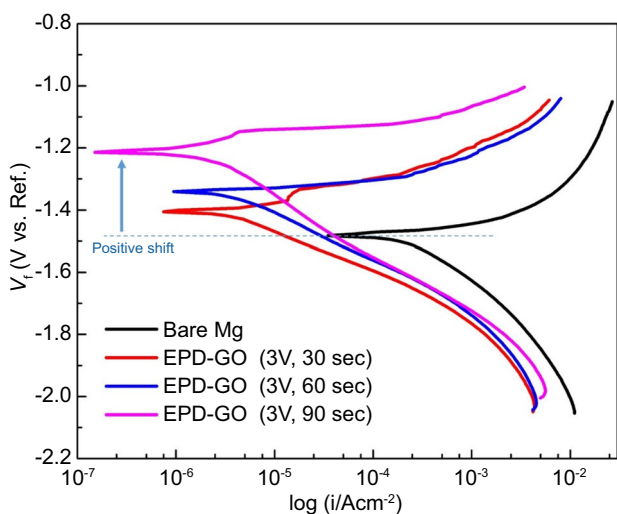


**Fig. 7: Tafel curves of bare Mg and EPD-GO (3 V at 30, 60, and 90 s) obtained in Ringer’s lactate**

**Table 1: Kinetic parameters obtained from Tafel fit**

Sample	$B_a$ (mV/decade)	$B_c$ (mV/decade)	$i_{corr}$ ( $\mu\text{A}/\text{cm}^2$ )	$E_{corr}$ (V)	Avg. Corrosion rate (mpy)
Bare Mg	101.5	315.9	$36.40 \pm 0.63$	- 1.48	32.39
EPD-GO (3 V, 30 s)	81.00	147.0	$4.290 \pm 0.057$	- 1.40	4.056
EPD-GO (3 V, 60 s)	51.00	167.7	$4.580 \pm 0.039$	- 1.34	3.707
EPD-GO (3 V, 90 s)	128.4	209.4	$2.260 \pm 0.021$	- 1.21	2.004

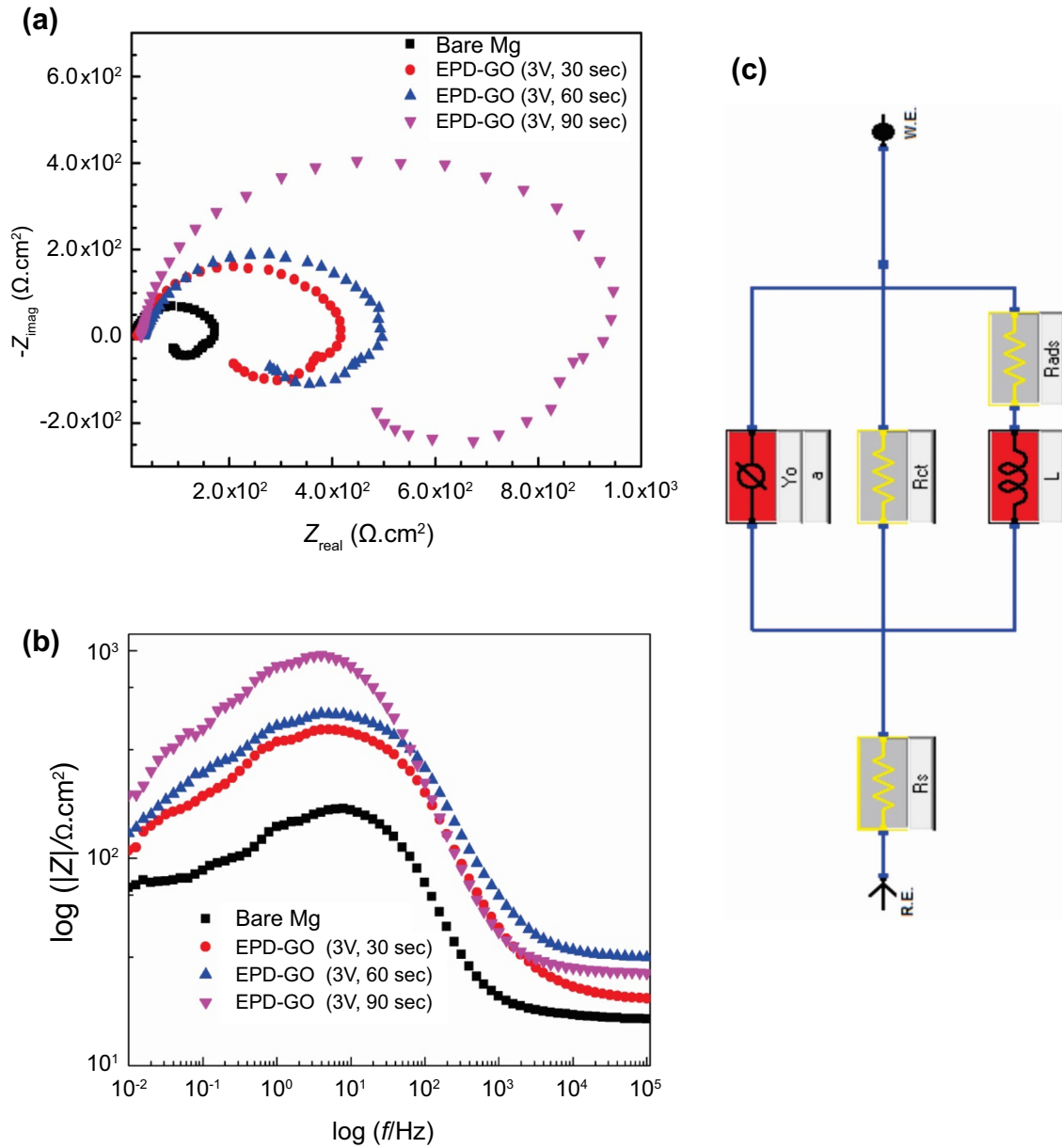


Fig. 8: a Nyquist plot, b Bode plot of bare Mg and EPD-GO (3 V, 30, 60, and 90 s)-coated Mg samples obtained in Ringer’s lactate, and c ECC model used for bare Mg and EPD-GO samples

Table 2: Impedance values obtained from the fitting of Nyquist curves

Sample	$R_s$ (Ω*cm <sup>2</sup> )	$R_{ct}$ (Ω*cm <sup>2</sup> )	$R_{rad}$ (Ω*cm <sup>2</sup> )	$L$ (H*cm <sup>2</sup> )	$Y_0$ (μS*s <sup>a</sup> /cm <sup>2</sup> )	$n$
Bare Mg	17.36	151.3	94.34	64.20	33.50	0.92
EPD-GO (3 V, 30 s)	21.87	378.3	174.2	243.5	16.80	0.85
EPD-GO (3 V, 60 s)	33.72	436.5	210.1	306.9	11.8	0.86
EPD-GO (3 V, 90 s)	28.96	873.5	299.2	708.3	10.41	0.93

## Conclusions

GO was successfully produced by improved Hummers' method and was found to have a thickness of 0.7–1 nm as determined by AFM analysis. GO coatings were successfully deposited on Mg alloys from an ultrasonicated GO–water suspension through EPD technique. XRD curves of the Mg-coated sample confirm the presence of GO on Mg samples after EPD coating. SEM analysis revealed GO coating provided good coverage to Mg. Tafel analysis in Ringer's lactate solution showed  $\sim 16\times$  drop in corrosion rate of EPD-GO (3 V, 90 s) than the bare alloy. Tafel results were well validated by EIS analysis. GO coatings produced in this work have a potential in maneuvering the degradation rate of AZ31B Mg alloys for biomedical application.

## References

1. Brusciotti, F, Snihirova, DV, Xue, H, Montemor, MF, Lamaka, SV, Ferreira, MG, "Hybrid Epoxy–Silane Coatings for Improved Corrosion Protection of Mg Alloy." *Corrosion Science*, **67** 82–90 (2013)
2. Hu, R-G, Zhang, S, Bu, J-F, Lin, C-J, Song, G-L, "Recent Progress in Corrosion Protection of Magnesium Alloys by Organic Coatings." *Progress in Organic Coatings*, **73** (2) 129–141 (2012)
3. Gao, R, Liu, Q, Wang, J, Zhang, X, Yang, W, Liu, J, Liu, L, "Fabrication of Fibrous Szaibelyite with Hierarchical Structure Superhydrophobic Coating on AZ31 Magnesium Alloy for Corrosion Protection." *Chemical Engineering Journal*, **241** 352–359 (2014)
4. Chen, X-B, Zhou, X, Abbott, TB, Easton, MA, Birbilis, N, "Double-Layered Manganese Phosphate Conversion Coating on Magnesium Alloy AZ91D: Insights into Coating Formation, Growth and Corrosion Resistance." *Surface and Coatings Technology*, **217** 147–155 (2013)
5. Yang, J, Cui, F, Lee, IS, "Surface Modifications of Magnesium Alloys for Biomedical Applications." *Annals of Biomedical Engineering*, **39** (7) 1857–1871 (2011)
6. Heublein, B, Rohde, R, Kaese, V, Niemeyer, M, Hartung, W, Haverich, A, "Biocorrosion of Magnesium Alloys: A New Principle in Cardiovascular Implant Technology?" *Heart*, **89** (6) 651–656 (2003)
7. Staiger, MP, Pietak, AM, Huadmai, J, Dias, G, "Magnesium and its Alloys as Orthopedic Biomaterials: A Review." *Biomaterials*, **27** (9) 1728–1734 (2006)
8. Chen, Q, Thouas, GA, "Metallic Implant Biomaterials." *Materials Science and Engineering: R: Reports*, **87** 1–57 (2015)
9. Razavi, M, Fathi, M, Savabi, O, Vashaei, D, Tayebi, L, "In Vivo Assessments of Bioabsorbable AZ91 Magnesium Implants Coated with Nanostructured Fluorinated Hydroxyapatite by MAO/EPD Technique for Biomedical Applications." *Materials Science and Engineering: C*, **48** 21–27 (2015)
10. Asl, VZ, Zhao, J, Anjum, MJ, Wei, S, Wang, W and Zhao, Z, "The Effect of Cerium Cation on the Microstructure and Anti-Corrosion Performance of LDH Conversion Coatings on AZ31 Magnesium Alloy." *Journal of Alloys and Compounds*, **821** 153248 (2020)
11. Chaya, A, Yoshizawa, S, Verdelis, K, Myers, N, Costello, BJ, Chou, D-T, Pal, S, Maiti, S, Kumta, PN, Sfeir, C, "In Vivo Study of Magnesium Plate and Screw Degradation and Bone Fracture Healing." *Acta Biomaterialia*, **18** 262–269 (2015)
12. Neupane, MP, Lee, S, Kang, J, Park, IS, Bae, TS, Lee, MH, "Surface Characterization and Corrosion Behavior of Silanized Magnesium Coated with Graphene for Biomedical Application." *Materials Chemistry and Physics*, **163** 229–235 (2015)
13. Hoche, H, Groß, S, Oechsner, M, "Development of New PVD Coatings for Magnesium Alloys with Improved Corrosion Properties." *Surface and Coatings Technology*, **259** 102–108 (2014)
14. Kang, Z, Lai, X, Sang, J, Li, Y, "Fabrication of Hydrophobic/Super-Hydrophobic Nanofilms on Magnesium Alloys by Polymer Plating." *Thin Solid Films*, **520** (2) 800–806 (2011)
15. Gray, J, Luan, B, "Protective Coatings on Magnesium and its Alloys—A Critical Review." *Journal of Alloys and Compounds*, **336** (1) 88–113 (2002)
16. Chen, F, Zhou, H, Yao, B, Qin, Z, Zhang, Q, "Corrosion Resistance Property of the Ceramic Coating Obtained Through Microarc Oxidation on the AZ31 Magnesium Alloy Surfaces." *Surface and Coatings Technology*, **201** (9) 4905–4908 (2007)
17. Hornberger, H, Virtanen, S, Boccaccini, A, "Biomedical Coatings on Magnesium Alloys—A Review." *Acta Biomaterialia*, **8** (7) 2442–2455 (2012)
18. Prabhu, DB, Gopalakrishnan, P, Ravi, K, "Morphological Studies on the Development of Chemical Conversion Coating on Surface of Mg–4Zn Alloy and its Corrosion and Biomineralisation Behaviour in Simulated Body Fluid." *Journal of Alloys and Compounds*, **812** 152146 (2020)
19. Geim, AK, Novoselov, KS, "The Rise of Graphene." *Nature Materials*, **6** (3) 183–191 (2007)
20. Liang, S, Shen, Z, Yi, M, Liu, L, Zhang, X, Ma, S, "In-Situ Exfoliated Graphene for High-Performance Water-Based Lubricants." *Carbon*, **96** 1181–1190 (2016)
21. Vicarelli, L, Heerema, SJ, Dekker, C, Zandbergen, HW, "Controlling Defects in Graphene for Optimizing the Electrical Properties of Graphene Nanodevices." *ACS Nano*, **9** (4) 3428–3435 (2015)
22. Ettore, V, De Marco, P, Zara, S, Perrotti, V, Scarano, A, Di Crescenzo, A, Petrini, M, Hadad, C, Bosco, D, Zavan, B, "In Vitro and In Vivo Characterization of Graphene Oxide Coated Porcine Bone Granules." *Carbon*, **103** 291–298 (2016)
23. Kotov, NA, "Materials Science: Carbon Sheet Solutions." *Nature*, **442** (7100) 254–255 (2006)
24. Cui, G, Bi, Z, Zhang, R, Liu, J, Yu, X and Li, Z, "A Comprehensive Review on Graphene-Based Anti-Corrosive Coatings." *Chemical Engineering Journal*, **373** 104–121 (2019)
25. Prasai, D, Tuberquia, JC, Harl, RR, Jennings, GK, Bolotin, KI, "Graphene: Corrosion-Inhibiting Coating." *ACS Nano*, **6** (2) 1102–1108 (2012)
26. An, SJ, Zhu, Y, Lee, SH, Stoller, MD, Emilsson, T, Park, S, Velamakanni, A, An, J, Ruoff, RS, "Thin Film Fabrication and Simultaneous Anodic Reduction of Deposited Graphene Oxide Platelets by Electrophoretic Deposition." *The Journal of Physical Chemistry Letters*, **1** (8) 1259–1263 (2010)
27. He, W, Zhu, L, Chen, H, Nan, H, Li, W, Liu, H, Wang, Y, "Electrophoretic Deposition of Graphene Oxide as a Corrosion Inhibitor for Sintered NdFeB." *Applied Surface Science*, **279** 416–423 (2013)
28. Raza, MA, Rehman, ZU, Ghauri, FA, Ahmad, A, Ahmad, R, Raffi, M, "Corrosion Study of Electrophoretically



- Deposited Graphene Oxide Coatings on Copper Metal.” *Thin Solid Films*, **620** 150–159 (2016)
29. Marcano, DC, Kosynkin, DV, Berlin, JM, Sinitskii, A, Sun, Z, Slesarev, A, Alemany, LB, Lu, W, Tour, JM, “Improved Synthesis of Graphene Oxide.” *ACS Nano*, **4** (8) 4806–4814 (2010)
  30. Nekahi, A, Marashi, P, Haghshenas, D, “Transparent Conductive Thin Film of Ultra Large Reduced Graphene Oxide Monolayers.” *Applied Surface Science*, **295** 59–65 (2014)
  31. Takadoun, J, Bennani, HH, “Influence of Substrate Roughness and Coating Thickness on Adhesion, Friction and Wear of TiN Films.” *Surface and Coatings Technology*, **96** (2) 272–282 (1997)
  32. Saud, SN, Bakhsheshi-Rad, H, Yaghoubidoust, F, Iqbal, N, Hamzah, E, Ooi, CR, “Corrosion and Bioactivity Performance of Graphene Oxide Coating on TiNb Shape Memory Alloys in Simulated Body Fluid.” *Materials Science and Engineering: C*, **68** 687–694 (2016)
  33. Gao, F, Xu, C, Hu, H, Wang, Q, Gao, Y, Chen, H, Guo, Q, Chen, D, Eder, D, “Biomimetic Synthesis and Characterization of Hydroxyapatite/Graphene Oxide Hybrid Coating on Mg Alloy with Enhanced Corrosion Resistance.” *Materials Letters*, **138** 25–28 (2015)
  34. Peng, F, Zhang, D, Wang, D, Liu, L, Zhang, Y and Liu, X, “Enhanced Corrosion Resistance and Biocompatibility of Magnesium Alloy by Hydroxyapatite/Graphene Oxide Bilayer Coating.” *Materials Letters*, **264** 127322 (2020)
  35. Soliman, H, Qian, J, Tang, S, Chen, Y, Makhlof, A-S, Wan, G, “Hydroxyquinoline/Nano-Graphene Oxide Composite Coating of Self-Healing Functionality on Treated Mg Alloys AZ31.” *Surface and Coatings Technology*, **385** 125395 (2020)
  36. Macdonald, JR, “Impedance Spectroscopy: Emphasizing Solid Materials and Systems.” *Applied Optics*, **28** 1083 (1989)
  37. Jamesh, MI, Wu, G, Zhao, Y, McKenzie, DR, Bilek, MM, Chu, PK, “Electrochemical Corrosion Behavior of Biodegradable Mg–Y–RE and Mg–Zn–Zr Alloys in Ringer’s Solution and Simulated Body Fluid.” *Corrosion Science*, **91** 160–184 (2015)
  38. Ghauri, FA, Raza, MA, Baig, MS and Ibrahim, S, “Corrosion Study of the Graphene Oxide and Reduced Graphene Oxide-Based Epoxy Coatings.” *Materials Research Express*, **4** 125601 (2017)
  39. Anjum, MJ, Zhao, J, Asl, VZ, Yasin, G, Wang, W, Wei, S, Zhao, Z, Khan, WQ, “In-Situ Intercalation of 8-Hydroxyquinoline in Mg–Al LDH Coating to Improve the Corrosion Resistance of AZ31.” *Corrosion Science*, **157** 1–10 (2019)

**Publisher’s Note** Springer Nature remains neutral with regard to jurisdictional claims in published maps and institutional affiliations.